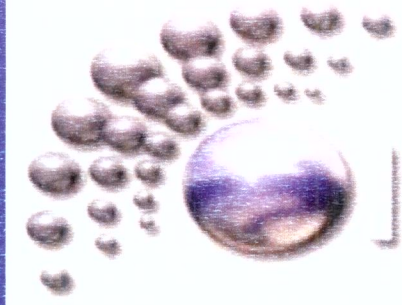

Abstracta

Ano VII- N. 05

Out.05

TRABALHOS PUBLICADOS

Agosto à Setembro 2005

P 209-05 à P 253- 05

TRABALHOS PUBLICADOS

P 209- 05 "Adsorption of phosphoric acid on niobium oxide coated cellulose fiber: Preparation, characterization and ion exchange property"

Pavan, F. A., Francisco, M. S. P., Landers, R., and Gushikem, Y.

The preparation procedures for a hybrid organic-inorganic cellulose-niobium oxide (Cel/Nb2O5) and its derivative, Cel/Nb2O5/phosphate, are described. The precursor reagent of the metal oxide was the very convenient water soluble niobium oxalate compound, NH4[NbO(C2O4)(2))(H2O)(2)].nH(2)O. Phosphate ion was adsorbed on the Cel/Nb2O5 by immersing this solid in an aqueous solution of phosphoric acid. Textural analyses carried out by using scanning electron microscopy (SEM) connected to an energy dispersive detector (EDS) revealed that the niobium oxide particles are, within the magnification used, uniformly dispersed on the cellulose matrix surface. Phosphoric acid is adsorbed on the material surface through the Nb-O-P linkage. The X-ray photoelectron and P-31 NMR spectra showed that the adsorbed phosphate on the surface is the (H2PO4)(-) species. The ion exchange isotherms obtained using the material Cel/Nb2O5/H2PO4- showed good affinity for retaining Na+, K+ and Ca2+ when in contact with these ions in an aqueous solution

Journal of the Brazilian Chemical Society 16[4], 815-820. 2005.

P 210- 05 "Characterization and quantification of symmetric Gaussian-state entanglement through a local classicality criterion"

de Oliveira, M. C.

A necessary and sufficient condition for characterization and quantification of entanglement of any bipartite Gaussian state belonging to a special symmetry class is given in terms of classicality measures of one-party states. For Gaussian states whose local covariance matrices have equal determinants it is shown that separability of a two-party state and classicality of a one-party state are completely equivalent to each other under a nonlocal operation, allowing entanglement features to be understood in terms of any available classicality measure

Physical Review A 72[1]. 2005.

P 211- 05 "Charge transfer effects in acid treated single-wall carbon nanotubes"

Barros, E. B., Souza, A. G., Lemos, V., Mendes, J., Fagan, S. B., Herbst, M. H., Rosolen, J. M., Luengo, C. A., and Huber, J. G.

Single-wall carbon nanotubes (SWNTs) prepared by the arc discharge method were oxidized using nitric acid. The samples were analyzed by using Raman scattering and Fourier transformed infrared spectroscopy (FTIR). The FTIR results indicate the presence of -COOH acid groups in the treated samples. The up shifts observed in the radial breathing mode frequencies suggest that SWNTs behave as donors after the acid treatment, with charge transfer occurring from the nanotubes to the -COOH groups. Ab initio calculations of SWNTs interacting with -COOH acid groups support the charge transfer process from the nanotubes to the carboxyl groups. (C) 2005 Elsevier Ltd. All rights reserved

Carbon 43[12], 2495-2500. 2005.

P 212- 05 "Co (II) porphyrin adsorbed on SiO2/SnO2/phosphate prepared by the sol-gel method"

Cardoso, W. S., Francisco, M. S. P., Landers, R., and Gushikem, Y.

This paper describes the immobilization procedure of 5,10,15,20-tetrakis(1-methyl-4-pyridyl)-21-H,23-H-porphyrin ion on SiO2/SnO2/ phosphate, obtained by the sol-gel processing method. P 2p X-ray photoelectron and the P-31 MAS NMR spectra revealed that dihydrogen phosphate is the species present on the surface. The porphyrin was adsorbed on the surface of the modified material and furthermore metallized in situ with Co (H) ion. The porphyrin metallation process was followed with UV-vis spectroscopy by inspecting the Q bands of the free and metallated porphyrin. The free porphyrin presented four Q bands associated to a D-2h local symmetry and the metallated one, two bands related to a D-4h local symmetry. The amount of electroactive species adsorbed on the material was estimated by integrating the area under the peak of Co (II) -> Co (I) reduction by using the pulse differential voltammetric technique.

The amount of the metallated porphyrin was 2.3 x 10(-10) Mol cm(-2). A carbon paste electrode of the modified material containing metallated porphyrin was used to study the electrocatalytic reduction of dissolved dioxygen by means of cyclic voltammetry, chronoamperometry and linear sweeping voltammetry. The modified electrode was very stable and exhibited the electrocatalytic reduction of dissolved dioxygen at -180mV versus SCE by a two-electron mechanism, producing hydrogen peroxide at pH 5.4. The electroactive species was strongly retained on the material surface, presumably inside the pores of the material, since in a test of various oxidation-reduction cycles no significant decrease of the current densities was detected, indicating that it was not leached off during the experiment.

Electrochimica Acta 50[22], 4378-4384. 2005.

P 213- 05 "Comment on "a/[110] stacking fault model for platelets in diamond" - Response"

Miranda, C. R., Antonelli, A., and Nunes, R. W.

Physical Review Letters 95[13]. 2005.

P 214- 05 "Core-shell CdS/Cd(OH)(2) quantum dots: synthesis and bioconjugation to target red cells antigens"

De Farias, P. M. A., Santos, B. S., De Menezes, F. D., Ferreira, R. D., Barjas-Castro, M. D., Castro, V., Lima, P. R. M., Fontes, A., and Cesar, C. L.

We report a new and efficient methodology of labelling red blood cells, in order to investigate the expression of anti-A antigen, employing luminescent semiconductor nanocrystals. Highly luminescent and stable core-shell cadmium sulphide/cadmium hydroxide [CdS/CdS(OH)(2)] colloidal particles were obtained in the nanometre size range. The surface of these particles was characterized by using a monoclonal anti-A antibody via a one-step glutaraldehyde cross-linking procedure, followed by conjugation of the particles to red cells of blood groups A(+), A(2)(+) and O+. Laser scanning confocal microscopy images indicated that after conjugation for 30 min, A(+) and A(2)(+) erythrocytes presented different patterns of dual bright emission whereas the O+ group cells showed no emission. We suggest that this labelling procedure may be applied as a quantitative tool to investigate the distribution and expression of alloantigen in red blood cells

Journal of Microscopy-Oxford 219, 103-108. 2005.

P 215- 05 "Diagnosis of thyroid multinodular goiter using diffraction-enhanced imaging"

Rocha, H. S., Lopes, R. T., Valiante, P. M., Tirao, G., Mazzaro, I., Honnicke, M. G., Cusatis, C., and Giles, C.

Diffraction-enhanced images (DEI) have been obtained using two silicon crystals. A first channel-cut silicon crystal using the Si(3 3 3) reflection is employed to reduce the divergence of the pre-monochromated Si(l 1 1) beam of the light line to 60 microradian (12 arcsec). A second channel-cut Si(3 3 3) crystal was used as a Bragg analyzer to obtain bright and dark field images by changing its angular position. This technique is ideally suited for soft-tissue imaging or objects with the same absorption coefficient interfaces. DEI was developed at the XRD-2 beamline at the Brazilian Synchrotron (LNLS) in Campinas-Brazil. Feasibility tests on acquired images, which allow the diagnosis of thyroid nodular goiter, were performed. This disease is ordinary. The tissue developed on the cervical area causes compression of the nearby structures and undesirable aesthetic deformities with worldwide distribution. DEI of the tissues were taken to observe their morphology and to compare with the microscopic analysis (histopathological). This technique allows cutting sections a hundred times thicker than conventional histological techniques allowing a complete vision of the disease morphology. DEI show details not clearly seen with conventional techniques.

Nuclear Instruments & Methods in Physics Research Section A-Accelerators Spectrometers Detectors and Associated Equipment 548[1-2], 175-180. 2004.

TRABALHOS PUBLICADOS

P 216- 05 "Diffraction-enhanced imaging for studying pattern recognition in cranial ontogeny of bats and marsupials"

Rocha, H. S., Lopes, R. T., Pessoa, L. M., Honnicke, M. G., Tirao, G., Cusatis, C., Mazzaro, I., and Giles, C

The key to understanding evolution lies in the elucidation of mechanisms responsible for the observed underlying patterns and in the observation of sequences that emerge from those evolutionary landmarks. The comparative development can be used to access the derivation of form and the homology versus the convergence of evolution features. Phylogenetic and biological homologies are necessary to discern the evolutionary origins of these features. This work examined the patterns of cranial formation in pre-born bat specimens as well as post-born opossum by means of microradiography and Diffraction-Enhanced Radiography (DER) techniques. A direct conversion CCD camera was used to provide micrometer spatial resolution in order to acquire highly detailed density images. This technique allows the observation of structures, in early stages of development, which were impossible to be observed with traditional techniques, such as clearing and staining. Some cranial features have been described for adults in the literature, but the detailed description of the appearance sequence of those features in these species is still unknown and obscure. Microradiography and diffraction-enhanced imaging can improve quality of morphological detail analysis and permit the identification of anatomical landmarks that are useful in comparative studies and are still unknown in both species. In this study, we access evolution features in cranial morphology of bats and marsupials using both X-ray techniques. (c) 2005 Elsevier B.V. All rights reserved

***Nuclear Instruments & Methods in Physics Research Section A-Accelerators Spectrometers Detectors and Associated Equipment* 548[1-2], 228-233. 2004.**

P 217- 05 "Diffuse component spectra of solar active regions at submillimeter wavelengths"

Silva, A. V. R., Lagana, T. F., De Castro, C. G. G., Kaufmann, P., Costa, J. E. R., Levato, H., and Rovira, M.

Solar maps at 212 and 405 GHz obtained by the Solar Submillimetric Telescope (SST) show regions of enhanced brightness temperature, which coincide with the location of active regions. A statistical study of the radio emission from these active regions was performed for the first time at such high frequencies during 23 days on June and July 2002, when the atmospheric opacity was low. The brightest regions on the maps were chosen for this study, where the brightness excess observed varies from 3 to 20% above quiet Sun levels (i.e., 200-1000 K) at both wavelengths. Sizes of the regions of enhanced emission calculated at half the maximum value were estimated to be between 2' and 7'. These sizes agree with observed sizes of active regions at other wavelengths such as H alpha and ultraviolet. An important result is that the flux density spectra of all sources increase toward submillimeter frequencies, yielding flux density spectral index with an average value of 2.0. The flux density of the active region sources were complemented with that from maps at 17 and 34 GHz from the Nobeyama Radio Heliograph. The resulting spectra at all four frequencies were fit considering the flux density to be due to thermal bremsstrahlung from the active region. In the calculations, the source radius was assumed to be the mean of the measured values at 212 and 405 K. The effective temperatures of the radio emitting source, assumed homogeneous, obtained from this fit were 0.6-2.9 x 10(4) K, for source diameters of 2'-7'

***Solar Physics* 227[2], 265-281. 2005.**

P 218 - 05 "Dipolar-biased giant magnetoimpedance"

Sinnecker, J. P., de Araujo, A. E. P., Piccin, R., Knobel, M., and Vazquez, M.

The effect of the dipolar field on the magnetoimpedance in Fe- and Co-based wires is presented. In the experiments a Co-based wire was used as a probe to measure the giant magnetoimpedance (GMI), while a Fe-based wire was employed to generate the dipolar field. The GMI curve showed a shift in the anisotropy field and a highly asymmetric profile. The dipole-dipole interaction can be employed to design novel linear GMI sensors and to properly tune their field operation. (C) 2005 Elsevier B.V. All rights

***Journal of Magnetism and Magnetic Materials* 295[2], 121-125. 2005.**

P 219 - 05 "Direct near infrared photorefractive recording and pre-exposure controlled hole-electron competition with enhanced recording in undoped Bi12TiO20"

dos Santos, P. V., Frejlich, J., and Carvalho, J. F.

We report the direct recording of electron-based photorefractive hologram in nominally undoped Bi12TiO20 crystals using 780 nm wavelength light without pre-exposure or any kind of previous processing. A lower intensity absorption grating is also detected. Pre-exposure with shorter wavelength produces an extended lifetime hole-based complementary grating on another photoactive center level and leads to enhanced recording

***Applied Physics B-Lasers and Optics* 81[5], 651-655. 2005.**

P 220 - 05 "Disorder and the effective Mn-Mn exchange interaction in Ga1-xMnxAs diluted magnetic semiconductors"

da Silva, A. J. R., Fazzio, A., dos Santos, R. R., and Oliveira, L. E.

We perform a theoretical study, using ab initio total energy density-functional calculations, of the effects of disorder on the Mn-Mn exchange interactions for Ga1-xMnxAs diluted magnetic semiconductors. For a 128 atoms supercell, we consider a variety of configurations with 2, 3, and 4 Mn atoms, which correspond to concentrations of 3.1%, 4.7%, and 6.3%, respectively. In this way, the disorder is intrinsically considered in the calculations. Using a Heisenberg Hamiltonian to map the magnetic excitations, and ab initio total energy calculations, we obtain the effective J(n)(Mn-Mn), from first (n=1) all the way up to sixth (n=6) neighbors. Calculated results show a clear dependence in the magnitudes of the J(n)(Mn-Mn) with the Mn concentration x. Also, configurational disorder and/or clustering effects lead to large dispersions in the Mn-Mn exchange interactions, in the case of fixed Mn concentration. Moreover, theoretical results for the ground-state total energies for several configurations indicate the importance of a proper consideration of disorder in treating temperature and annealing effects

***Physical Review B* 72[12]. 2005.**

P 221- 05 "Double-pumped fiber optical parametric amplifier with flat gain over 47-nm bandwidth using a conventional dispersion-shifted fiber"

Boggio, J. M. C., Marconi, J. D., and Fragnito, H. L.

We investigate the performance of conventional. dispersion-shifted fibers (DSFs). as nonlinear medium in double-pumped fiber, optical parametric amplifiers (2P-FOPAs). We report on high gain (37 dB) with low ripple (+/- 1.5 dB) over a 47-mn bandwidth using these fibers. We show that the 2P-FOPA average gain, and the gain. uniformity are limited. by longitudinal variations of the zero dispersion wavelength and by polarization-Mode dispersion. We demonstrate that 2P-FOPAs constructed with DSFs exhibit negligible crosstalk even for high gains (40 dB) and-large output signal powers (12.5 dBm) in a ten-channel system

***Ieee Photonics Technology Letters* 17[9], 1842-1844. 2005.**

P 222- 05 "Effects of hydrostatic pressure and applied electric fields on the exciton states in GaAs-(Ga,Al)As quantum wells"

Raigoza, N., Duque, C. A., Reyes-Gomez, E., and Oliveira, L. E.

The effects of both hydrostatic pressure and electric fields applied perpendicular to the layers on the direct-exciton states in single GaAs-(Ga,Al)As quantum wells are studied. Theoretical calculations are performed within the variational procedure, in the framework of the effective-mass and non-degenerate parabolic-band approximations. Both heavy- and light-hole exciton energies and corresponding quantum-confined Bohr radii are obtained. The pressure coefficient is also theoretically evaluated and found in good agreement with available experimental measurements. (c) 2005 Elsevier B.V. All rights reserved

***Physica B-Condensed Matter* 367[1-4], 267-274. 2005.**

P 223- 05 "Effects of laser irradiation and annealing on rhodium phthalocyanine Langmuir-Blodgett films"

Gaffo, L., Brasil, M. J. S. P., Cerdeira, F., and Moreira, W. C.

The effects of laser irradiation and annealing of rhodium phthalocyanine Langmuir-Blodgett films deposited on quartz and Au-covered glass substrates were studied with ultraviolet-visible and Fourier transform infrared spectroscopy, X-ray diffraction and atomic force microscopy. We found that laser irradiation and annealing produce very similar results attributed to the heating effect in both cases and produce different results in different atmospheres (air and Helium). Changes observed in, films treated, at 200 degrees C in an inert atmosphere are attributed to a molecular rearrangement of the films associated with the destruction of J aggregates. Films treated in similar conditions in air show, besides this effect, possible oxidation and loss of molecules. A remarkable decrease of toughness was observed when the films are annealed at 100 degrees C in He, attributed to the evaporation of water molecules trapped in the Langmuir-Blodgett films.

Thin Solid Films **488[1-2], 236-241. 2005.**

P 224- 05 "Elastic scattering of low-energy electrons by OCS (vol 70, pg 062711, 2004)"

Bettega, M. H. F., Lima, M. A. P., and Ferreira, L. G.

In a previous publication [Phys. Rev. A. 70, 062711 (2004)] we presented results for electron collisions with OCS molecules. We found a Pi shape resonance and discussed the existence of an s-wave virtual state through the analysis of the scattering length. The existence of the Pi shape resonance has been reported by other theoretical and experimental studies, and the existence of an s-wave virtual state has been suggested by an experimental study. In this Addendum we show that besides the Pi shape resonance and the s-wave virtual state, this molecule also presents a Ramsauer-Townsend minimum around 1 eV

Physical Review A **72[1]. 2005.**

P 225 - 05 "Electron collisions with CS2"

Bettega, M. H. F., Lima, M. A. P., and Ferreira, L. G.

We present elastic integral and differential cross sections for electron collisions with CS2 molecules for energies up to 10 eV. To compute the cross sections we employed the Schwinger multichannel method implemented with pseudopotentials at the static-exchange plus polarization approximation. In particular, our integral cross section shows a sharp increase near zero energy, which is an indication of the existence of an s-wave virtual state, followed by a Ramsauer-Townsend minimum around 0.7 eV. Our results agree well with available experimental and theoretical results

Journal of Physics B-Atomic Molecular and Optical Physics **38[13], 2087-2095. 2005.**

P 226- 05 "Emission of thermally activated electrons from rare gas clusters irradiated with intense VUV light pulses from a free electron laser"

Laarmann, T., Rusek, M., Wabnitz, H., Schulz, J., de Castro, A. R. B., Gurtler, P., Laasch, W., and Moller, T.

The ionization dynamics of Ar and Xe clusters irradiated with intense vacuum ultraviolet light from a free-electron laser is investigated using photoelectron spectroscopy. Clusters comprising between 70 and 900 atoms were irradiated with femtosecond pulses at 95 nm wavelength (similar to 13 eV photon energy) and a peak intensity of similar to 4x10(12) W/cm(2). A broad thermal distribution of emitted electrons from clusters with a maximum kinetic energy up to 30-40 eV is observed. The observation of relatively low-energy photoelectrons is in good agreement with calculations using a time-dependent Thomas-Fermi model and gives experimental evidence of an outer ionization process of the clusters, due to delayed thermoelectronic emission

Physical Review Letters **95[6]. 2005.**

P 227- 05 "Hydrogen etching mechanism in nitrogen implanted iron alloys studied with in situ photoemission electron spectroscopy"

Figueroa, C. A. and Alvarez, F.

In situ photoemission electron spectroscopy (XPS) is used to elucidate the hydrogen etching mechanism in nitrogen implanted iron alloys. The samples were prepared by bombarding stainless steel with a broad nitrogen ion source in a high vacuum chamber. The photoemission spectra evolution on increasing hydrogen ion current is correlated with the nitrided surface properties. The presence of hydrogen is associated with oxygen removal, augmenting the surface nitrogen concentration. The total active sites at the surface are constant, i.e., oxygen competes with nitrogen sites on the surface. The absorbed oxygen is etched following a linear law on hydrogen ion flux. Simultaneously, the formation of metallic nitrides is enhanced. At the working temperature, the efficiency of the process is determined by a characteristic time that depends on hydrogen retention time, water formation and desorption time.

Journal of Vacuum Science & Technology A 23[5], L9-L12. 2005.

P 228- 05 "Influence of a dynamical gluon mass in the pp and (p)over-bar-p forward scattering"

Luna, E. G. S., Martini, A. F., Menon, M. J., Mihara, A., and Natale, A. A.

We compute the tree level cross section for gluon-gluon elastic scattering taking into account a dynamical gluon mass, and show that this mass scale is a natural regulator for this subprocess cross section. Using an eikonal approach in order to examine the relationship between this gluon-gluon scattering and the elastic pp and (p) over barp channels, we found that the dynamical gluon mass is of the same order of magnitude as the ad hoc infrared mass scale m(0) underlying eikonalized QCD-inspired models. We argue that this correspondence is not an accidental result, and that this dynamical scale indeed represents the onset of nonperturbative contributions to the elastic hadron-hadron scattering. We apply the eikonal model with a dynamical infrared mass scale to obtain predictions for sigma(tot)(pp,(p) over barp), rho(pp,(p) over barp), slope B-pp,B-(p) over barp, and differential elastic scattering cross section d sigma((p) over barp)/dt at Tevatron and CERN-LHC energies

Physical Review D **72[3]. 2005.**

P 229- 05 "Infrared studies on films of carbosilazane and siloxazane networks"

Trasferetti, B. C., Gelamo, R. V., Rouxinol, F. P., de Moraes, M. A. B., and Davanzo, C. U.

The present work describes the effects of diluting hexamethyldisilazane (HMDSN) vapor either in pure argon or in oxygen-argon mixtures on the solid film deposited from the resulting plasma. Such a dilution provides a manner of incorporating controllable amounts of Si-O groups into the solid film. The characterization of the films investigated here was made by longitudinal and transverse optical (LO and TO, respectively) functions in the mid-infrared calculated through the Kramers-Kronig analysis of transmittance spectra. The infrared analysis showed that the films were formed by silicon-centered distorted tetrahedra of the following type: Si(CH3)(x)BU(2-0.5x), where 0 <= x <= 3 and BU stands for bridging unit. For the sample deposited in the absence of O-2 in the discharge, BU = CH2 and NH; for the samples deposited with an O-2 flow rate (f(O2)) of 2.5 and 10 sccm, BU = CH2, NH, and O; and for the sample deposited with f(O2) of 20 sccm, BU = NH and O. The Delta(LO-TO) for the Si-O asymmetrical stretching increased from 0 (f(O2) = 0 sccm) to 73 cm(-1) (f(O2) = 20 sccm), while for the Si-N asymmetrical stretching it decreased from 20 (f(O2) = 0 sccm) to 3 cm(-1) (f(O2) = 20 sccm). These observations signal an increase in the Si-O-Si network and a decrease in the Si-NH-Si network as the oxygen flow increased. An interesting conclusion drawn from our analysis of the Si-H stretching mode position and Delta(LO-TO) for the AS1 band is that the films deposited in the presence of O-2 are not structurally homogeneous, but have domains with different proportions of O bridges

Chemistry of Materials **17[18], 4685-4692. 2005.**

P 230- 05 "Kramers equation for a charged Brownian particle: The exact solution"

Simoes, T. P. and Lagos, R. E.

We report the exact fundamental solution for Kramers equation associated to a Brownian gas of charged particles, under the influence of homogeneous (spatially uniform) otherwise arbitrary, external mechanical, electrical and magnetic fields. Some applications are presented, namely the hydrothermodynamical picture for Brownian motion in the long-time regime. (c) 2005 Elsevier B.V. All rights reserved

Physica A-Statistical Mechanics and Its Applications **355[2-4], 274-282. 2005.**

P 231- 05 "Lattice distortion effects on the magnetostructural phase transition of MnAs"

Iikawa, F., Brasil, M. J. S. P., Adriano, C., Couto, O. D. D., Giles, C., Santos, P. V., Daweritz, L., Rungger, I., and Sanvito, S.

We present a systematic experimental and theoretical study of the first-order phase transition of epitaxially grown MnAs thin films under biaxial tensile stress. Our results give direct information on the dependence of the phase-transition temperature of MnAs films on the lattice parameters. We demonstrate that an increase of the lattice constant in the hexagonal plane raises the phase-transition temperature (T-p), while an increase of the perpendicular lattice constant lowers T-p. The results of calculations based on density functional theory are in good agreement with the experimental ones. Our findings open exciting prospects for magneto-mechanical devices, where the critical temperature for ferromagnetism can be engineered by external stress

Physical Review Letters **95[7]. 2005.**

P 232- 05 "Monte Carlo simulations applied to AlxGayIn(1-x-y)X quaternary alloys (X=As,P,N): A comparative study"

Marques, M., Ferreira, L. G., Teles, L. K., and Scolfaro, L. M. R

We develop a different Monte Carlo approach applied to the A(x)B(y)C(1-x-y)D quaternary alloys. Combined with first-principles total-energy calculations, the thermodynamic properties of the (Al,Ga,In)X (X=As, P, or N) systems are obtained and a comparative study is developed in order to understand the roles of As, P, and N atoms as the anion X in the system AlxGayIn1-x-yX. Also, we study the thermodynamics of specific compositions in which AlGaInN, AlGaInP, and AlGaInAs are lattice matched, respectively, to the GaN, GaAs, and InP substrates. We verify that the tendency for phase separation is always towards the formation of an In-rich phase. For arsenides and phosphides this occurs in general for lower temperatures than for their usual growth temperatures. This makes these alloys very stable against phase separation. However, for nitrides the In and/or Al concentrations have to be limited in order to avoid the formation of In-rich clusters and, even for low concentrations of In and/or Al, we observe a tendency of composition fluctuations towards the clustering of the ternary GaInN. We suggest that this latter behavior can explain the formation of the InGaN-like nanoclusters recently observed in the AlGaInN quaternary alloys

Physical Review B **71[20]. 2005.**

P 233 - 05 "Nonadditivity of decoherence rates in superconducting qubits"

Burkard, G. and Brito, F.

We show that the relaxation and decoherence rates T-1(-1) and T-2(-1) of a qubit coupled to several noise sources are in general not additive, i.e., that the total rates are not the sums of the rates due to each individual noise source. To demonstrate this, we calculate the relaxation and pure dephasing rates T-1(-1) and T-phi(-1) of a superconducting (SC) flux qubit in the Born-Markov approximation in the presence of several circuit impedances Z(i) using network graph theory and determine their deviation from additivity (the mixing term). We find that there is no mixing term in T-phi(-1) and that the mixing terms in T-1(-1) and T-2(-1) can be positive or negative, leading to reduced or enhanced relaxation and decoherence times T-1 and T-2. The mixing term due to the circuit inductance L at the qubit transition frequency omega(01) is generally of second order in omega(01)L/Z(i), but of third order if all impedances Z(i) are pure resistances. We calculate T-1,T-2 for an example of a SC flux qubit coupled to two impedances

Physical Review B **72[5]. 2005.**

P 234- 05 "Nonlinear transport properties of III-nitrides in electric field"

Rodrigues, C. G., Vasconcellos, A. R., Luzzi, R., and Freire, V. N.

We consider the transport properties of polar direct-gap semiconductors in an electric field, specializing the numerical calculation of the general theory to the case of n-doped III-nitrides, in particular, GaN, AlN, and InN. The nonequilibrium thermodynamic state of these materials-characterized by the variables so-called quasitemperature, quasichemical potential, and drift velocity of the carriers, and the quasitemperatures of longitudinal optical and acoustical phonons-is studied. The evolution equations of these variables-which are highly nonlinear-are derived, and the transient regime and the ensuing steady state are analyzed. The nonlinear transport is characterized and its main properties are discussed. In one case comparison with a recent Monte Carlo calculation is made and good agreement is obtained. In this paper we mainly consider the ultrafast transient, and in the following paper the steady state. (c) 2005 American Institute of Physics

Journal of Applied Physics **98[4]. 2005.**

P 235- 05 "Nonlinear transport properties of doped III-N and GaAs polar semiconductors: A comparison"

Rodrigues, C. G., Vasconcellos, A. R., Luzzi, R., and Freire, V. N.

In the previous article we have presented a study of the transport properties of doped direct-gap inverted-band polar semiconductors III-nitrides and GaAs in the steady state, calculated with a nonlinear quantum transport theory based on a nonequilibrium ensemble formalism. In the present one such results are compared with calculations using Monte Carlo-modeling simulations and with experimental measurements. Materials of the n-type and p-type dopings in the presence of intermediate to high electric fields, and for several temperatures of the external reservoir, are considered. The agreement between the results obtained using the nonlinear quantum kinetic theory, with those of Monte Carlo calculations and experimental data is remarkably good, thus satisfactorily validating this powerful, concise, and physically sound formalism. (c) 2005 American Institute of Physics

Journal of Applied Physics **98[4]. 2005.**

P 236- 05 "Optical and structural investigation of In1-xGaxP free-standing microrods"

Nakaema, M. K. K., Godoy, M. P. F., Brasil, M. J. S. P., Iikawa, F., Silva, D., Sacilotti, M., Decobert, J., and Patriarche, G.

We present a structural and optical characterization of scepterlike micrometer-sized free-standing structures, composed of a long InGaP rod with a metallic sphere on its top, grown on polycrystalline InP substrates. In contrast to the conventional vapor-liquid-solid growth method, no catalyst was deposited on the substrate. Instead, metallic In liberated from the InP substrate by phosphor evaporation works as the catalyst metal. We performed Raman scattering, photoluminescence spectroscopy, scanning electron microscopy, and energy dispersive x-ray spectroscopy measurements on individual structures. The alloy composition measured by microscopic techniques is in agreement with the values obtained by the optical measurements considering that the rod is strain free. The InGaP rods present essentially constant Ga composition within a fluctuation of similar to 10% and efficient optical emission. We also observed a marked increase in the Raman-scattering signal at rod positions near the metallic sphere (the "neck"), which was attributed to a surface-enhanced Raman-scattering effect. Our results demonstrate the possibility of using InGaP rods for optical device applications. (c) 2005 American Institute of Physics

Journal of Applied Physics **98[5]. 2005.**

P 237- 05 "Photoionization of helium atoms irradiated with intense vacuum ultraviolet free-electron laser light. Part I. Experimental study of multiphoton and single-photon processes"

Laarmann, T., de Castro, A. R. B., Gurtler, P., Laasch, W., Schulz, J., Wabnitz, H., and Moller, T.

The interaction of He atoms with intense vacuum-ultraviolet light of a free-electron laser is investigated using time-of-flight mass spectroscopy and photoelectron spectroscopy. The atoms were irradiated with 100 fs pulses at 95 nm wavelength, which corresponds to similar to 13 eV photon energy. The ionization of He atoms is observed at a peak intensity of 10(10)-10(13) W/cm(2), which is due both to nonlinear multiphoton ionization with the fundamental wavelength and single-photon ionization with third harmonic radiation of the free-electron laser. The observation of two sharp photoelectron peaks in the kinetic energy spectra, that are separated by the photon energy, is in agreement with the numerical solution of the time-dependent Schrodinger equation. The calculation was done using the fully quantized field and a limited but representative set of basis states. The ionization rate dependence on the laser peak intensity indicates that: (a) The low-energy peak in the photoelectron spectra is mainly due to two-photon absorption of the fundamental, but (b) the high-energy peak at 15.4 eV is probably due to third harmonic FEL radiation. The theoretically predicted contribution from three-photon absorption of the fundamental is of about the same order of magnitude and could not be separated from the third harmonic background signal. Particularly, the photoelectron spectra and He+ time-of-flight data give evidence that the intensity of third harmonic light is high enough to perform single-shot spectroscopy on gas phase samples

***Physical Review A* 72[2]. 2005.**

P 238 -05 "Photoionization of helium atoms irradiated with intense vacuum ultraviolet free-electron laser light. Part II. Theoretical modeling of multi-photon and single-photon processes"

de Castro, A. R. B., Laarmann, T., Schulz, J., Wabnitz, H., and Moller, T.

We consider the problem of a helium atom under the radiation field of the DESY vacuum ultraviolet (VUV) free electron laser (FEL) (Phase I, h congruent to 13 eV). We find by solving numerically the time-dependent Schrodinger equation, that there is a large probability for resonant two-photon excitation from the ground state into a low kinetic energy state just above the first He ionization threshold. From this it is possible to go into another quasi-free state higher up, by resonant absorption of an additional photon. There is no double ionization of He. These results are in general agreement with the He photoelectron and time-of-flight (TOF) spectra recorded on March 2002, in the last week of the DESY VUV FEL Phase I operation. A detailed report on the experiments is given in a companion paper

***Physical Review A* 72[2]. 2005.**

P 239 -05 "Plasma confinement using biased electrode in the TCABR tokamak"

Nascimento, I. C., Kuznetsov, Y. K., Severo, J. H. F., Fonseca, A. M. M., Elfimov, A., Bellintani, V., Machida, M., Heller, M. V. A. P., Galvao, R. M. O., Sanada, E. K., and Elizondo, J. I.

Experimental data obtained on the TCABR tokamak (R = 0.61 m, a = 0.18 m) with an electrically polarized electrode, placed at r = 0.16 m, is reported in this paper. The experiment was performed with plasma current of 90 kA (q = 3.1) and hydrogen gas injection adjusted for keeping the electron density at 1.0 x 10(19) m(-3) without bias. Time evolution and radial profiles of plasma parameters with and without bias were measured. The comparison of the profiles shows an increase of the central line-averaged density, up to a maximum factor of 2.6, while H alpha hydrogen spectral line intensity decreases and the C III impurity stays on the same level. The analysis of temporal behaviour and radial profiles of plasma parameters indicates that the confined plasma enters the H-mode regime. The data analysis shows a maximum enhanced energy confinement factor of 1.95, decaying to 1.5 at the maximum of the density, in comparison with predicted Neo-Alcator scaling law values. Indications of transient increase of the density gradient near the plasma edge were obtained with measurements of density profiles. Calculations of turbulence and transport at the Scrape-Off-Layer, using measured floating potentials and ion saturation currents, show a strong decrease in the power spectra and transport. Bifurcation was not observed and the decrease in the saturation current occurs in 50 mu s

***Nuclear Fusion* 45[8], 796-803. 2005.**

P 240 - 05 "Quantum transport properties of a two-channel atomic-sized magnetic contact"

Dartora, C. A. and Cabrera, G. G.

We propose a simple model to theoretically study the conductance of atomic-sized magnetic contacts. Our approach considers in detail the case of two-atom contacts with two spin channels, and the conductance is calculated using Landauer theory in the ballistic regime. For ferromagnetic contacts, we examine the large magnetoresistance effect obtained, when changing the magnetic configuration of the leads from parallel to antiparallel. We also discuss nonmagnetic transition metals nanocontacts, where conductance measurements display a behavior similar to magnetic contacts. Our treatment of the above phenomena reveals the important role played by quantum fluctuations in the contact region

***Physical Review B* 72[6]. 2005.**

P 241- 05 "Rabi oscillations in two-level semiconductor systems"

Brandi, H. S., Latge, A., Barticevic, Z., and Oliveira, L. E.

Rabi oscillation, in coherent optical excitations in bulk GaAs and quantum dot two-level systems may be converted into deterministic photocurrents, with the impurities or dots providing the tag for each qubit. Here we perform a theoretical analysis of the damping of Rabi oscillations in two-level semiconductor systems. Present calculations, through optical Bloch equations on excitonic two-level InxGa1-xAs quantum-dot systems, are found in good agreement with the corresponding experimental data. Calculated results indicate that the nature underlying the dephasing mechanism associated to the damping of the measured Rabi oscillations, which has previously remained as an open question, may be associated with a field-dependent recombination rate related to the inhomogeneous broadening of the excitonic lines in the InxGa1-xAs two-level QD system.

***Solid State Communications* 135[6], 386-389. 2005.**

P 242- 05 "Raman, hyper-Raman, hyper-Rayleigh, two-photon luminescence and morphology-dependent resonance modes in a single optical tweezers system"

Fontes, A., Ajito, K., Neves, A. A. R., Moreira, W. L., de Thomaz, A. A., Barbosa, L. C., de Paula, A. M., and Cesar, C. L.

We present a setup of optical tweezers combined with linear and nonlinear microspectroscopies that enhances the capabilities of capture and analysis of both techniques. We can use either a continuous-wave (cw) Ti:sapphire laser for Raman measurements or a pulsed femtosecond Ti:sapphire laser that permitted the observation of nonlinear results such as hyper-Raman, hyper-Rayleigh, and two-photon luminescence. Only the high peak intensity of the femtosecond laser allows the observation of all these nonlinear spectroscopies. The sensitivity of our system also permitted the observation of morphology-dependent resonance (MDR) modes of a single stained trapped microsphere of 6 mu m. The possibility of performing spectroscopy in a living microorganism optically trapped in any desired neighborhood would mean that one can dynamically observe the chemical reactions and/or mechanical properties changing in real time

***Physical Review e* 72[1]. 2005.**

P 243- 05 "Sequencing-independent delocalization in a DNA-Like double chain with base pairing"

Caetano, R. A. and Schulz, P. A.

The question of whether or not DNA is intrinsically conducting is still a challenge. The ongoing debate on DNA molecules as an electronic material has so far underestimated a key distinction of the system: the role of base pairing in opposition to correlations along each chain. We show that a disordered base paired double chain presents truly or, at least, effectively delocalized states. This effect is irrespective to the sequencing along each chain

***Physical Review Letters* 95[12]. 2005.**

P 244- 05 "Spin-dependent transmission coefficients for magnetic tunnel junctions: Transport properties and temperature dependence"

Dartora, C. A. and Cabrera, G. G.

In this paper we present a detailed analysis of the spin-dependent transmission coefficients for magnetic tunnel junctions (MTJ's) including magnon scattering dependence. The conduction electrons are modeled as plane waves and the electron-magnon interaction in the interfaces can be treated as a perturbation opening the spin-flip conduction channels. We explore the main transport properties of the MTJ such as bias and temperature dependence of conductance and magnetoresistance. Our theory is in good agreement with experimental data

Physical Review B 72[1]. 2005.

P 245- 05 "Spin-excitations of the quantum Hall ferromagnet of composite fermions"

Doretto, R. L., Goerbig, M. O., Lederer, P., Caldeira, A. O., and Smith, C. M.

The spin excitations of a fractional quantum Hall system are evaluated within a bosonization approach. In a first step, we generalize Murthy and Shankar's Hamiltonian theory of the fractional quantum Hall effect to the case of composite fermions with an extra discrete degree of freedom. Here, we mainly investigate the spin degrees of freedom, but the proposed formalism may be useful also in the study of bilayer quantum-Hall systems, where the layer index may formally be treated as an isospin. In a second step, we apply a bosonization scheme, recently developed for the study of the two-dimensional electron gas, to the interacting composite-fermion Hamiltonian. The dispersion of the bosons, which represent quasiparticle-quasihole excitations, is analytically evaluated for fractional quantum Hall systems at nu=1/3 and nu=1/5. The finite width of the two-dimensional electron gas is also taken into account explicitly. Furthermore, we consider the interacting bosonic model and calculate the lowest-energy state for two bosons. In addition to a continuum describing scattering states, we find a bound-state of two bosons. This state is interpreted as a pair excitation, which consists of a skyrmion of composite fermions and an antiskyrmion of composite fermions. The dispersion relation of the two-boson state is evaluated for nu=1/3 and nu=1/5. Finally, we show that our theory provides the microscopic basis for a phenomenological nonlinear sigma model for studying the skyrmion of composite fermions

Physical Review B 72[3]. 2005.

P 246- 05 "Strong orbital correlations in a Fe-substituted spin-glass-manganite"

Granado, E., Urbano, R. R., Perez, C. A., Azimonte, C., Lynn, J. W., Souza, R. A., Souza-Neto, N. M., Ramos, A. Y., Bychkov, G. L., Shiryaev, S. V., and Barilo, S. N..

The compound La0.66Ba0.40Mn0.61Fe0.33O3 shows anisotropic magnetic correlations with no long-range order. Specific heat measurements suggest these correlations represent the bulk. Orbital correlations of Mn(3+)e(g) electrons, surviving in an environment of largely disordered exchange interactions, are invoked to account for this magnetic state. These results argue in favor of a strain-field mechanism for orbital ordering in manganites

Physical Review B 72[5]. 2005.

P 247- 05 "Structure of habit-modifying trivalent transition metal cations (Mn3+, Cr3+) in nearly perfect single crystals of potassium dihydrogen phosphate as examined by X-ray standing waves, X-ray absorption spectroscopy, and molecular modeling"

Lai, X. J. and Roberts, K. J.

The local atomic structure of habit-modifying transition metal cations within the crystal lattice of potassium dihydrogen phosphate (KDP) is investigated using X-ray absorption spectroscopy (XAS) and X-ray standing wave (XSW) spectroscopy, together with molecular modeling. XAS reveals the transition metal cations to be structurally incorporated into the crystal lattice as an ionic complex that is octahedrally coordinated to two phosphate groups and four water molecules. The position of transition metal cation, as determined by XSW, is consistent with its location at an interstitial lattice site, with a coherent position 0.66 with respect to the 12001 crystal lattice planes. The structural model suggested that the transition metal complex mimics the surface structure of KDP prismatic {100} face, hence facilitating its adsorption on this face. Charge compensation associated with the impurity incorporation during crystal growth is effected via the hydrated impurity complex displacing one bonding proton that binds two phosphate groups together with two potassium ions within the crystal structure to maintain the system charge balance. The resulting model is consistent with the XAS and XSW results as well as earlier work (Barrett, N.; Lamble, G. M.; Roberts, K. J.; Sherwood, J. N.; Greaves, G. N.; Davey, R. J.; Oldman, R. J.; Jones, D. J. Cryst. Growth 1989, 94, 689), albeit contrasting with our preliminary data on the isomorphous ammonium dihydrogen phosphate in which a substitutional model was proposed (Cunningham, D. A. H.; Hammond, R. B.; Lai, X.; Roberts, K. J. Chem. Mater. 1995, 7 (9), 1690)

Chemistry of Materials 17[16], 4053-4061. 2005.

P 248- 05 "The effect of nanocrystal surface structure on the luminescence properties: Photoemission study of HF-etched InP nanocrystals"

Adam, S., Talapin, D. V., Borchert, H., Lobo, A., McGinley, C., de Castro, A. R. B., Haase, M., Weller, H., and Moller, T.

InP nanocrystals with narrow size distribution and mean particle diameter tunable from similar to 2 up to similar to 7 nm were synthesized via the dehalosilylation reaction between InCl3 and tris(trimethylsilyl)phosphine. Specific capping of the nanocrystal surface with a shell of organic ligands protects the nanocrystals from oxidation and provides solubility of the particles in various organic solvents. InP nanocrystals with enhanced photoluminescence (PL) efficiency were obtained from the initial nanocrystals by photoassisted etching of the nanocrystal surface with HF. The resulting PL quantum efficiency of InP nanocrystals dispersed in n-butanol is about three orders of magnitude higher when compared to the nonetched InP samples and approaches similar to 40% at room temperature. High-resolution photoelectron spectroscopy with the use of synchrotron radiation was applied to reveal the changes of the nanocrystal surface responsible for the dramatic improvement of the PL efficiency. The analysis of high-resolution P 2p core-level spectra confirmed significant changes of the nanocrystal surface structure induced by the postpreparative treatments and allowed us to propose the description of the etching mechanism. In the nonetched InP nanocrystals, some surface P atoms generate energy states located inside the band gap which provide nonradiative recombination pathways. Photoassisted treatment of InP nanocrystals with HF results in selective removal of these phosphorous atoms from the nanocrystal surface. The reconstructed surface of the etched InP nanocrystals is terminated mainly with In atoms and is efficiently passivated with tri-n-octylphosphine oxide ligands. (c) 2005 American Institute of Physics

Journal of Chemical Physics 123[8]. 2005.

P 249- 05 "The electric pield outside and inside a resistive spherical shell carrying a steady azimuthal current"

Hernandes, J. A. and Assis, A. K. T.

We calculate the potential, electric field and surface charges outside and inside a resistive spherical shell carrying a steady azimuthal Current. We obtain a time-independent electric field different from zero in both regions

Physica Scripta 72[2-3], 212-217. 2005.

P 250 - 05 "Time-resolved thermal lens measurements of the thermo-optical properties of glasses at low temperature down to 20 K"

Astrath, N. G. C., Rohling, J. H., Medina, A. N., Bento, A. C., Baesso, M. L., Jacinto, C., Catunda, T., Lima, S. M., Gandra, F. G., Bell, M. J. V., and Anjos, V.

In this work the time resolved thermal lens spectrometry was applied to measure the absolute values of the thermo-optical properties of low silica calcium aluminosilicate and soda lime glasses at low temperatures, in the range between 20 and 300 K. The thermal relaxation calorimetry was used as a complementary technique to determine the specific heat. The results showed a marked decrease of the thermal diffusivity with the temperature rise, with a dependence similar to that of the mean free path (similar to T-1) in the interval between 20 and 70 K, while in the range between 70 and 300 K the dependence was T-(0.33 +/- 0.02). The marked variation of the temperature coefficient of the optical path length change with the temperature rise was attributed to the increase in the coefficient of the electronic polarizability. The results also showed that for the aluminosilicate glass the excess in the specific heat correlated to the so-called boson peak occurred at about 17 K, higher than that of soda lime, which occurs at about 12 K. In conclusion, our results showed the ability of the time resolved thermal lens to determine the thermo-optical properties of glasses at low temperatures, bringing possibilities for experiments in a wide range of optical materials

Physical Review B 71[21]. 2005.

P 251- 05 "Transport properties of an intermediate-valence model of Tl2Mn2O7"

Foglio, M. E. and Barberis, G. E.

The appearance of colossal magnetoresistance (CMR) in Tl2Mn2O7 has stimulated many recent studies of the pyrochlore family of compounds A(2)B(2)O(7). The double exchange model of Zener does not describe the CMR in Tl2Mn2O7, because its metallic conductivity cannot be explained by doping. Here we employ Hubbard operators to reformulate the intermediate valence model used by Ventura and Alascio [Phys. Rev. B 56, 14533 (1997)] to describe the electronic structure and transport properties of this compound. Following Foglio and Figueira [Phys. Rev. B 62, 7882, (2000)] we use approximate one-electron Green's functions to calculate the thermopower and the static and dynamic conductivity of Tl2Mn2O7 for several magnetic fields. A qualitative agreement was obtained with the experimental measurements of those properties. Although the agreement is far from perfect, these quantities are fairly well described by the same set of system parameters

Physical Review B 72[12]. 2005.

P 252- 05 "Two-photon absorption in CdTe quantum dots"

Padilha, L. A., Fu, J., Hagan, D. J., Van Stryland, E. W., Cesar, C. L., Barbosa, L. C., and Cruz, C. H. B.

We report measurements of frequency degenerate and nondegenerate two-photon absorption (2PA) spectra of CdTe quantum dots, QDs, in glass matrices and compare them with 2PA in bulk CdTe. We find that the 2PA is strongly dependent on the size of the QDs becoming smaller with decreasing size, even when normalizing to the volume of the dots. We adapt a simple degenerate 2PA model, based on the effective mass approximation, to nondegenerate 2PA, and this model correctly describes the experimental data for 2-photon energies up to similar to 1.4Eg. This suggests that, once the spectrum for one size of quantum dot is known, the model can be used for predicting the degenerate and nondegenerate 2PA spectra of different sized QDs of the same semiconductor. (c) 2005 Optical Society of America

Optics Express 13[17], 6460-6467. 2005.

P 253- 05 "Uniform approximation for the coherent-state propagator using a conjugate application of the Bargmann representation"

Ribeiro, A. D., Novaes, M., and de Aguiar, M. A. M.

We propose a conjugate application of the Bargmann representation of quantum mechanics. Applying the Maslov method to the semiclassical connection formula between the two representations, we derive a uniform semiclassical approximation for the coherent-state propagator which is finite at phase space caustics

Physical Review Letters 95[5]. 2005.

Abstracta

Instituto de Física "Gleb Wataghin"
Universidade Estadual de Campinas - UNICAMP
Diretor: Prof. Dr. Júlio César Hadler Neto
Cidade Universitária C.P. 6165
CEP: 13081-970 - Campinas - SP - Brasil
e-mail: secdir@ifi.unicamp.br
Fone: 0XX 19 3788-5300 / Fax: 0XX 19 3788-3127

Publicação

Biblioteca do Instituto de Física "Gleb Wataghin"
site: http://www.ifi.unicamp.br/bif
Diretora Técnica: Rita Aparecida Sponchiado

Elaboração
Tânia Macedo Folegatti
abstract@ifi.unicamp.br

Projeto Gráfico
ÍgneaDesign

Impressão
Gráfica Central - Unicamp